[Article] www.whxb.pku.edu.cn

氧原子在具有 Pt 皮肤的 $Pt_3Ni(111)$表面的吸附和扩散

杨宗献[1,2,*] 于小虎[1] 马东伟[1]

([1] 河南师范大学物理与信息工程学院, 河南 新乡 453007; [2] 河南省光伏材料重点实验室, 河南 新乡 453007)

摘要： 用基于密度泛函理论的第一性原理方法研究了氧原子在具有 Pt 皮肤的 $Pt_3Ni(111)$[记为 Pt-skin-$Pt_3Ni(111)$]表面的吸附和扩散特性. 重点研究了氧原子在 Pt-skin-$Pt_3Ni(111)$表面的扩散问题, 这对理解 Pt-skin-$Pt_3Ni(111)$催化剂的高催化活性有重要意义. 结果表明: 氧原子容易吸附在 fcc 位; 催化剂 Pt_3Ni 中的 Ni 原子对催化剂的电子结构有很大影响, 从而改变了其对氧原子的吸附. 用推拉弹性带(NEB)方法搜索氧原子的扩散势垒, 并解释了 Pt-skin-$Pt_3Ni(111)$催化剂的高催化活性.

关键词： 密度泛函理论; 氧原子; 扩散; Pt 皮肤; $Pt_3Ni(111)$表面

中图分类号： O641; O647

Adsorption and Diffusion of Oxygen Atom on $Pt_3Ni(111)$ Surface with Pt-Skin

YANG Zong-Xian[1,2,*] YU Xiao-Hu[1] MA Dong-Wei[1]

([1]*College of Physics and Information Engineering, Henan Normal University, Xinxiang 453007, Henan Province, P. R. China*; [2]*Henan Key Laboratory of Photovoltaic Materials, Xinxiang 453007, Henan Province, P. R. China*)

Abstract: The adsorption and diffusion properties of O atoms on the surface of $Pt_3Ni(111)$ with a Pt skin [denoted as "Pt-skin-$Pt_3Ni(111)$"] were studied by the first-principles method based on the density functional theory (DFT). Special attention was paid to the diffusion properties of the adsorbed oxygen on the Pt-skin-$Pt_3Ni(111)$ surface as this is important in understanding the high activity of the Pt-skin-$Pt_3Ni(111)$ catalyst. We found that O atoms prefered fcc binding sites. Ni atoms in the Pt_3Ni catalyst drastically influence the electronic configuration of the system and therefore the binding of oxygen atoms. Nudged elastic band (NEB) calculations were used to determine the diffusion barrier of oxygen atoms on the surface, providing a possible explanation for the distinct catalytic activity of the Pt-skin-$Pt_3Ni(111)$ catalyst.

Key Words: Density functional theory; Oxygen atom; Diffusion; Pt-skin; $Pt_3Ni(111)$ surface

The electronic structure of metal surface can be modified dramatically by doping the second metal on the surface or forming bimetallic catalysts which usually have improved activity, selectivity, and/or lifetimes compared to their pure counterparts. This gives a way to tune the properties of catalysts for the target reaction. Low-temperature fuel cells are attracting considerable interest as a means of producing electricity by direct electrochemical conversion of hydrogen and oxygen into water[1]. The catalysts on the anode and cathode are mainly made up of Pt. However, inadequate efficiency of energy conversion and the cost associated with Pt catalysts remain a cause of concern. To make low-temperature fuel cells economically viable, people are striving in developing new catalysts using less Pt but having better efficiency. One of the solutions is using the Pt-bimetallic alloys which have attracted much attention[2–13].

Various experimental[2–5] and theoretical[6–13] studies have been performed to achieve these goals by designing Pt-based alloy electrocatalysts. Experimentally, Stamenkovic *et al.*[2,3] reported

Received: May 15, 2009; Revised: July 17, 2009; Published on Web: September 9, 2009.

*Corresponding author. Email: yzx@henannu.edu.cn; Tel: +86-373-3329346.

The project was supported by the National Natural Science Foundation of China (10674042) and Henan Innovation Project for University Prominent Research Talents, China (2007KYCX004).

国家自然科学基金(10674042)和河南省高校杰出科研人才创新工程项目(2007KYCX004)资助

new materials with high catalytic activity, and found that Pt-skin-Pt_3Ni(111) catalyst was 10-fold more active for the oxygen reduction reaction (ORR) than the corresponding Pt(111) surface and 90-fold more active than the current state-of-art Pt/C catalysts for proton exchange membrane fuel cell (PEMFC)[2]. Mun *et al.*[4] studied the electronic structure of Pt_3M (M=Ti, V, Cr, Fe, Co, Ni) polycrystalline alloys with valence-band photoemission spectroscopy. They found that the surface segregation of Pt was the same as that predicted in the thermodynamic models, and the trends of the measured *d*-band centers for the annealed alloy surfaces were the same as those predicted by the density functional theory calculations. Markovic *et al.*[5] reported that bimetallic Pt_3M (M=Cr, Mn, Co) alloy catalysts could dramatically enhance the ORR reactivity as compared with the pure Pt. Further characterization revealed that the formation of the Pt overlayer (so called Pt skin) due to the segregation under operating conditions and the decrease in lattice constant by alloying were the main driven forces behind not only for the increasing number of active sites but also for the activity of adsorbates.

Theoretically, using the plane-wave DFT method, Zhang *et al.*[6] studied the catalytic activity of Pt-bimetallic systems with Pt-overlayers on different pure metal substrates and found that platinum monolayer had higher catalytic activity than pure Pt. Jacob *et al.*[7] studied the electronic structure and geometry structure of the PtNi alloy and the adsorption of H and O atoms on the alloy surface using a cluster model, and found that the bulk structure of Pt_3Ni alloy had the cubic close packed structure, and the oxygen or hydrogen atom bound more strongly on the PtNi alloy than on pure platinum. Kitchin *et al.*[10,11] studied how the combination of strain and ligand effects modified the surface electronic and chemical properties of the sandwiched Pt-3*d*-Pt structure. Nilekar *et al.*[12] studied Pt monolayer-based ORR catalysts using various experimental methods and first-principles density functional theory calculations, and found that the bimetallic and ternary alloys had improved catalytic activity for the oxygen reduction. Su *et al.*[8] presented a first-principles density functional theory investigation of the reactivity of Pt(111)-skin catalysts with different Ni concentrations in the substrate (Pt_xNi_{1-x}), and found that the interaction between adsorbates and substrates was weakened with increase in Ni because the down-shift of *d*-band center of surface Pt atoms, and activation barriers of CO and H oxidation toward atomic oxygen gradually decreased. Recently, using the DFT-based method and models for the Pt_3M (111) (M=Fe, Co, Ni) that are close to the highly active ORR catalyst: Pt-skin-Pt_3M(111) was found in the experiments[2,3], Ma *et al.* studied the surface segregation of Pt in bimetallic Pt_3M (M=Fe, Co, Ni) alloys[9] and the adsorption of atomic oxygen on Pt-segregated and nonsegregated surface of Pt_3M(111) (M=Fe, Co, Ni)[13].

The present study aimed at understanding why Pt-skin-Pt_3Ni (111) surface had the high catalytic activity, through analyzing the electronic structure of the Pt-skin-Pt_3Ni(111) surface, and studing adsorption and diffusion of oxygen on the surface of Pt-skin-Pt_3Ni(111). Special attention was paid to the diffusion properties of the adsorbed oxygen on the Pt-skin-Pt_3Ni(111) surface, which are keys to understanding the high activity of the Pt-skin-Pt_3Ni(111) catalyst.

1 Model and calculation methods

1.1 Description of the model systems

The bulk Pt_3Ni alloy was modeled by replacing one of the four Pt atoms in the cubic fcc unit cell with a Ni atom and then had a full relaxation. The calculated equilibrium lattice constants were 0.398, 0.352, and 0.388 nm for bulk Pt, Ni, and Pt_3Ni, respectively, which were consistent with the previous experimental (e.g., 0.392 and 0.352 nm for Pt and Ni, respectively[14]) and DFT studies (e.g., 0.396 nm[7], 0.398 nm[9,13,15], 0.400 nm[8,16] for pure Pt; 0.352 nm[17], 0.361 nm[7] for pure Ni; and 0.388 nm[9], 0.389 nm[7], 0.390 nm[8] for Pt_3Ni). The (111) surfaces of pure Pt, pure Ni, Pt_3Ni alloy were cleaved from their corresponding bulk and modeled by slabs including six atomic layers of metal atoms periodically repeated (in *z* direction) with 1.3 nm of vacuum separating the slabs as shown in Fig.1(a, b), where Fig.1(a) may represent the Pt(111) or the Ni(111) surface which has the same structure. A (2×2) surface (including four metal atoms each layer) was used for the pure Pt or Ni systems and surfaces of equivalent size were used for the alloy systems. In the slab of the Pt_3Ni alloy, there were three Pt atoms and one Ni atom on each layer as shown in Fig.1 (b). The Pt-skin-Pt_3Ni(111) was obtained by exchanging the Ni atom in the surface layer with one of the Pt atoms in the second layer as shown in Fig.1(c), which included a pure Pt top layer, a Pt_2Ni_2 alloy layer for the subsurface layer and Pt_3Ni alloy layers for all other lower layers. This model was reasonable and relevant since experimental and theoretical studies had shown that the formation of a Pt-skin layer was accompanied with a Pt-depleted layer underneath for many Pt-3*d* alloys[18-21]. Very recently, Stamenkovic *et al.*[2] examined the Pt_3Ni(111) surface and found that the first layer consisted only of Pt and the second layer was strongly Pt-depleted (48% of Pt compared to 75% of Pt in the bulk). Therefore, for the adsorption of oxygen on the surface of Pt_3Ni(111) alloy, only the Pt-skin-Pt_3Ni(111) system considered.

The atomic oxygen adsorbate was placed on one side of the relaxed slabs. Three layers at the bottom were fixed and the three top layers, as well as the adsorbate, were allowed to fully relax.

1.2 Calculations

Spin-polarized calculations were performed using the Vienna *ab initio* simulation package (VASP) program[22,23] based on the density functional theory. The projector-augmented wave (PAW) method[24] of Blöchl, as implemented in VASP, was used for the treatment of the core electrons, and the electrons of Pt 5*d*, 6*s,* Ni 3*d*, 4*s*, and O 2*s*, 2*p* were treated as valence electrons. The Kohn-Sham one-electron valence states were expanded in a plane-wave basis set with well converged kinetic cutoff at 400 eV. A Monkhorst-Pack (MP) method was used for the Brillouin

Zone sampling[25]. A 4×4×1 MP mesh was used for all the surface calculations. For the structure optimization, the ionic positions were allowed to relax until the Hellman-Feynman forces were less than 0.2 eV·nm^{-1}. These values have been found to give good convergence for the geometric structures and relative energies under consideration (e.g., binding energies and activation brarriers).

The *d*-band density of state was determined by projection of the planewaves onto spherical harmonic orbitals. The *d*-band center was calculated as the first moment of the projected *d*-band density of state on the surface atoms referenced to the Fermi level.

The adsorption energy (E_{ads}) was calculated as $E_{ads}=E_{slab}+E_O-E_{O/slab}$, which is the energy gain with respect to the adsorbates and the metal slab at infinite separation. Where $E_{O/slab}$ is the energy of a slab with an atomic O adsorbate (0.25 monolayer) at different sites. E_{slab} is the energy of a clean slab and E_O is the energy of an atomic O using a large cell with the dimensions of 0.8 nm×0.9 nm ×1.0 nm. Zero-point energies were not included in the calculations, since they are small and can hardly affect the results for the strong adsorption of oxygen. Here, a negative (positive) value represents endothermic (exothermic) adsorption.

The search of the transition state (TS) has been performed with the climbing-image nudge elastic band method (CI-NEB)[26], which allows calculation of the minimum energy path for an atomic rearrangement. In this study the rearrangement in question is referred to the diffusion of oxygen on a metal surface. The maximum of the diffusion energy profile gives the activation energy barrier to the diffusion.

2 Results and discussion

2.1 Energetics and geometric structure of oxygen adsorption

Four starting positions were considered for oxygen adsorption on the pure platinum surface as shown in Fig.1(a). The top (t) position has an oxygen atom sitting directly above the center of a surface platinum atom. The hcp (h) mode places the oxygen in a hollow site triangulated by three surface platinum atoms. There is a platinum atom in the second layer below the oxygen. Similarly the fcc (f) mode oxygen is in a hollow site triangulated by three surface platinum atoms with a platinum atom below the oxygen in the third layer. The bridge (b) mode places the oxygen half way between two adjacent platinum atoms. The same set of initial adsorption sites (t, h, f, b) are considered on pure Ni(111) surface.

On the Pt-skin-$Pt_3Ni(111)$, eight non-equivalent starting positions including two sets of the top, fcc, hcp, and bridge sites were considered. In Ma *et al.*'s work[13] the effect of Ni atom in the third layer was considered, so more positions were considered. However, we found that the effect of Ni atom in the third layer on the adsorption of oxygen atom was small, so we just considered the atoms in the first two layers when choosing the non-equivalent starting positions. The nomenclature becomes somewhat more complicated with the need to specify which type of atoms close to the adsorption site in the subsurface layer is involved in the adsorption mode. Here we define the two sets of adsorption sites as follows: T_1(PPN) denotes the top site with two Pt and one Ni neighbours in the subsurface layer, T_2(PNN) denotes the top site with one Pt and two Ni neighbours in the subsurface layer; F_1(PPN) denotes the fcc site with two Pt and one Ni neighbours in the subsurface layer, F_2(PNN) denotes the fcc site with one Pt and two Ni neighbours in the subsurface layer; H_1(N)

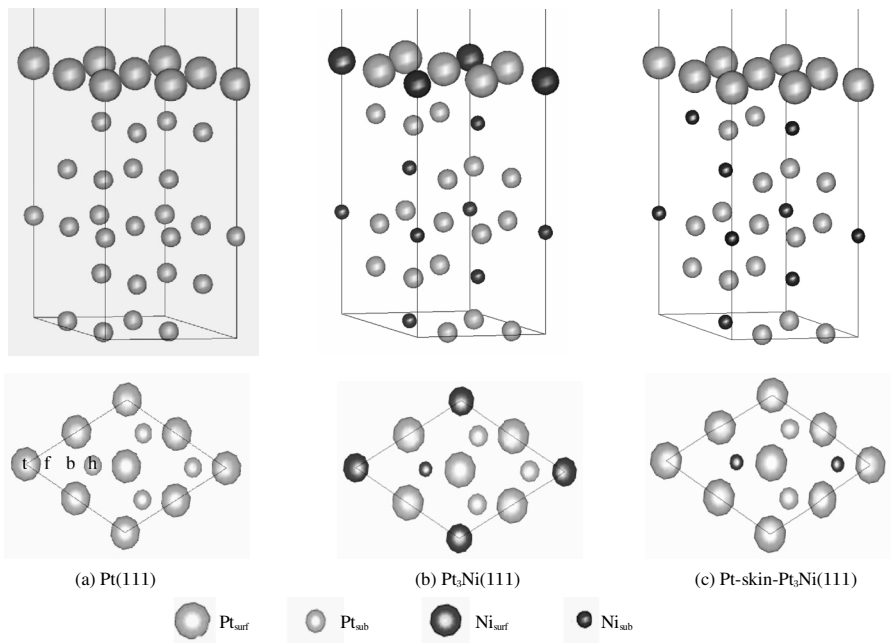

Fig.1 Side views and top views of the surfaces of (a) pure Pt(111), (b) $Pt_3Ni(111)$ alloy, and (c) Pt-skin-$Pt_3Ni(111)$

t: top, f: fcc, h: hcp, b: bridge

denotes the hcp site with one Ni neighbour in the subsurface layer, H_2(P) denotes the hcp site with one Pt neighbour in the subsurface layer. We do not distinguish the two bridge sites since they all converged to the neighbouring fcc site.

For pure Pt(111) surface, O is well-known to prefer to bind in the 3-fold hollow fcc sites[16,27]. Our calculated adsorption energies as well as the nearest O—Pt(Ni) distances for an oxygen atom on the pure Ni(111), pure Pt(111), and Pt-skin-Pt_3Ni(111) surfaces are shown in Table 1. It is found that for all the three surfaces, the bridge site adsorption does not exist since it converged to the neighbouring fcc site, therefore no bridge site entry is included in the table. The oxygen atom prefers to bind in the 3-fold hollow fcc sites and the binding strength follows the order of fcc>hcp> top.

On the pure Pt(111) surface, adsorption energy is 4.76 eV in the 3-fold hollow fcc site, whereas the adsorption energies on the hcp and top sites are 4.35 and 3.28 eV, respectively, which are about 0.41 and 1.48 eV lower than that on the fcc site. This agrees well with the experimental results [e.g., Gland *et al.*[23] determined an initial desorption energy of 4.77 eV for the Pt(111)/O system at 700 K, and Yeo *et al.*[29] reported a Pt—O bond energy of 4.32 eV on a clean Pt(111) surface] and the recent theoretical results [e.g., Ma *et al.*'s[13] DFT calculations gave the adsorption energies of 4.48, 4.05, and 3.14 eV for the fcc, hcp, and top sites, respectively; Han *et al.*'s[15] DFT calculations gave the adsorption energies of 4.67, 4.19, 3.08 eV for the fcc, hcp, and top sites, respectively; Xu *et al.*[16] found that the bridge site is actually a transition state for O diffusion, while the top site is considerably less stable]. On the pure Ni(111) surface, the adsorption is stronger than that on the Pt(111) surface. The favourable adsorption position for oxygen is the fcc site with an adsorption energy of 5.54 eV, which is followed by the adsorptions at the hcp and top sites with the adsorption energies of 5.44 and 3.56 eV, respectively.

On the Pt-skin-Pt_3Ni(111), there is a general trend that the site with more Ni neighbours in the subsurface layer has stronger adsorption between the sites of the same type [e.g., the strength orders of F_2(PNN)>F_1(PPN) and H_1(N)>H_2(P)]. Therefore, Ni neighbours in the subsurface layer play important roles in the oxygen adsorption on Pt-skin-Pt_3Ni(111). The most favourable position is the F_2(PNN) with an adsorption energy of 4.07 eV, while the F_1(PPN) has a lower adsorption energy (3.80 eV). The H_1(N) and H_2(P) come next with adsorption energies of 3.62 and 3.54 eV, respectively. The adsorption at the top sites has the lowest stability with the T_2(PNN) converged to the neighboring F_2(PNN) structure and T_1(PPN) with an adsorption energy of 2.79 eV. These results are in agreement with the recent DFT results of Ma *et al.*[13] which reported the values of 4.16, 3.91, 3.77, 3.61, and 2.97 eV for the sites corresponding to F_2(PNN), F_1(PPN), H_1(N), H_2(P), and T_1(PPN) in the present study, respectively.

Table 1 Adsorption energies (E_{ads}) as well as the nearest O—M (M=Ni or Pt) distance (d_{nn}) for an oxygen atom on the Ni(111), Pt(111), and Pt-skin-Pt_3Ni(111) surfaces

Surface	Site	E_{ads}/eV	d_{nn}/nm
Pt(111)	top	3.28	0.183
	fcc	4.76	0.204
	hcp	4.35	0.205
Ni(111)	top	3.56	0.166
	fcc	5.54	0.184
	hcp	5.44	0.184
Pt-skin-Pt_3Ni(111)	top	2.79(T_1)	0.184(T_1)
	fcc	3.80(F_1); 4.07(F_2)	0.205, 0.205, 0.206(F_2)
	hcp	3.62(H_1); 3.54(H_2)	0.207, 0.204, 0.207(H_1)

The labels in the brackets denote the adsorption sites (refer to the text).

Comparatively, the adsorption of oxygen on the Pt-skin-Pt_3Ni (111) is weaker than that on the either the pure Pt(111) or Ni(111) counterparts, indicating that the diffusion of oxygen would be easier on the Pt-skin-Pt_3Ni(111) surface. And this general trend can be easily explained by the *d*-band center theory[30,31]. Hammer and Nörskov[30] have shown that the interactions between adsorbates and transition metal surfaces involve the entire *d*-band, and the characteristics of the surface metal *d*-bands, particularly the weighted center of the *d*-band, plays a decisive role in determining surface reactivity. The first moment of the *d*-band is the average energy of the band, also called the *d*-band center (ε_d). The calculated first layer density of state (DOS) for the Pt(111) and Pt-skin-Pt_3Ni(111) surfaces and their corresponding *d*-band centers are shown in Fig.2, which shows that the first layer *d*-band center of Pt-skin-Pt_3Ni(111), −2.68 eV, is lower than that of Pt(111), −2.47 eV. Therefore the Pt-skin-Pt_3Ni(111) surface has a weaker interaction with oxygen than the pure Pt(111).

It is known that if oxygen binds too strongly to the cathode of a fuel cell, it could poison the surface and reduce its activity. On the other hand, if oxygen binds too weakly, the coverage of O adatoms may be too low for significant reaction to take place or dissociation could become activated. This can easily explain the reason why Pt is more adapt to be as catalyst than pure Ni, because O binds weaker on pure Pt than on pure Ni. Now that the oxygen adsorption on Pt-skin-Pt_3Ni(111) is weaker than that on pure Pt, the Pt-skin-Pt_3Ni(111) might be able to alleviate O poison and, therefore enhance the ORR process.

Geometrically, the O—Pt distances at different sites are listed in Table 1. Here, only the most favourable fcc adsorption sites are

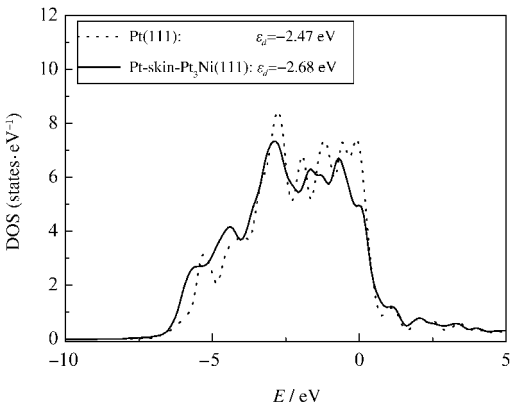

Fig.2 Surface *d*-band DOS for Pt(111) and Pt-skin-Pt_3Ni(111) surfaces with the calculated *d*-band center (ε_d) values

discussed. For oxygen adsorption on the fcc site of the Pt(111) surface, the calculated O—Pt bond length (d_{O-Pt}) is 0.204 nm which is similar to the previous DFT result of about 0.202 nm[32] and experimental value of 0.202 nm[33]. On pure Ni(111) surface, the calculated d_{O-Ni} is 0.184 nm, in agreement with the theoretical (0.186 nm)[34] and the experimental (0.185 nm)[35] values. For Pt-skin-$Pt_3Ni(111)$, the calculated d_{O-Pt} values on the F_2(PNN) site are 0.206, 0.205, 0.205 nm, respectively, which agree well with Ma *et al.*'s result (0.2053, 0.2065, 0.2075 nm)[13]. The different O—Pt(Ni) bond lengths on the different surfaces are correlated with their different adsorption strengths, i.e. the shorter the $d_{O-Pt(Ni)}$, the stronger the adsorption. The order of bond lengths of d_{O-Ni} (on Ni)<d_{O-Pt}(on Pt)<d_{O-Pt}[on Pt-skin-$Pt_3Ni(111)$] corresponds to the order of adsorption strengths of Ni(111)>Pt(111)>Pt-skin-$Pt_3Ni(111)$. O adsorption at the most favourable fcc sites induces a significant amount of perturbation on the Pt(111), Ni(111), Pt-skin-$Pt_3Ni(111)$ lattices. The Pt—Pt (or Ni—Ni) distances between the atoms neighbouring the O adatom are elongated by about 0.010 nm (on Pt), 0.006 nm (on Ni), 0.007 nm (0.008 nm, 0.009 nm) (on Pt-skin-Pt_3Ni) for the three surfaces, respectively. The distances between top two layers (d_{12}) before and after the O adsorption at the most favourable fcc site on Ni(111), Pt(111), and Pt-skin-$Pt_3Ni(111)$ are listed in Table 2. Before adsorption, the distances between the top two layers are about 0.201, 0.232, 0.225 nm, respectively, which agree well with Ma *et al.*' s result [13] (with the corresponding d_{12} values shown in brackets). With O adsorption, the distances between top two layers increase slightly by 0.004, 0.001, and 0.002 nm for the three surfaces, respectively. We notice an exception of our result (i.e., expansion of about 0.001 nm) to Ma *et al.*'s result[13] of the d_{12} value for O/Pt(111), where a slight contraction (by about 0.0011 nm) was reported.

Table 2 Calculated distances (d_{12}) between top two layers of Ni(111), Pt(111), and Pt-skin-$Pt_3Ni(111)$ surfaces with and without O adsorbate

Surface	d_{12}/nm	
	without O adsorbate	with O adsorbate
Ni(111)	0.201	0.205
Pt(111)	0.232 (0.2323)	0.233 (0.2312)
Pt-skin-$Pt_3Ni(111)$	0.225 (0.2238)	0.227 (0.2265)

The values in the bracket are from Ref.[13].

2.2 Diffusion of oxygen on the surface

Elastic band calculations were used to calculate the diffusion barriers for oxygen adatom moving across the Pt(111) and Pt-skin-$Pt_3Ni(111)$ surface. All possible diffusion routes between high symmetry sites were considered as shown in Fig.3. The calculations were carried out as a set of single "hop" between successive sites. On the Pt(111) surface, the hop from the fcc site (f) to the hcp site (h) is shown in Fig.3(a), with the start and end points of each hop indicated with the oxygen positions. It is clear that there is a transition state (TS) in the midway at the bridge position between the fcc site and hcp site with an energy barrier of 0.71 eV. On Pt-skin-$Pt_3Ni(111)$ surface a more complex series of hops (e.g. F_1-H_1-F_2-H_2-F_3) were calculated as shown in Fig.3(b). The maximum barrier (TS) of 0.65 eV occurs at the bridge position

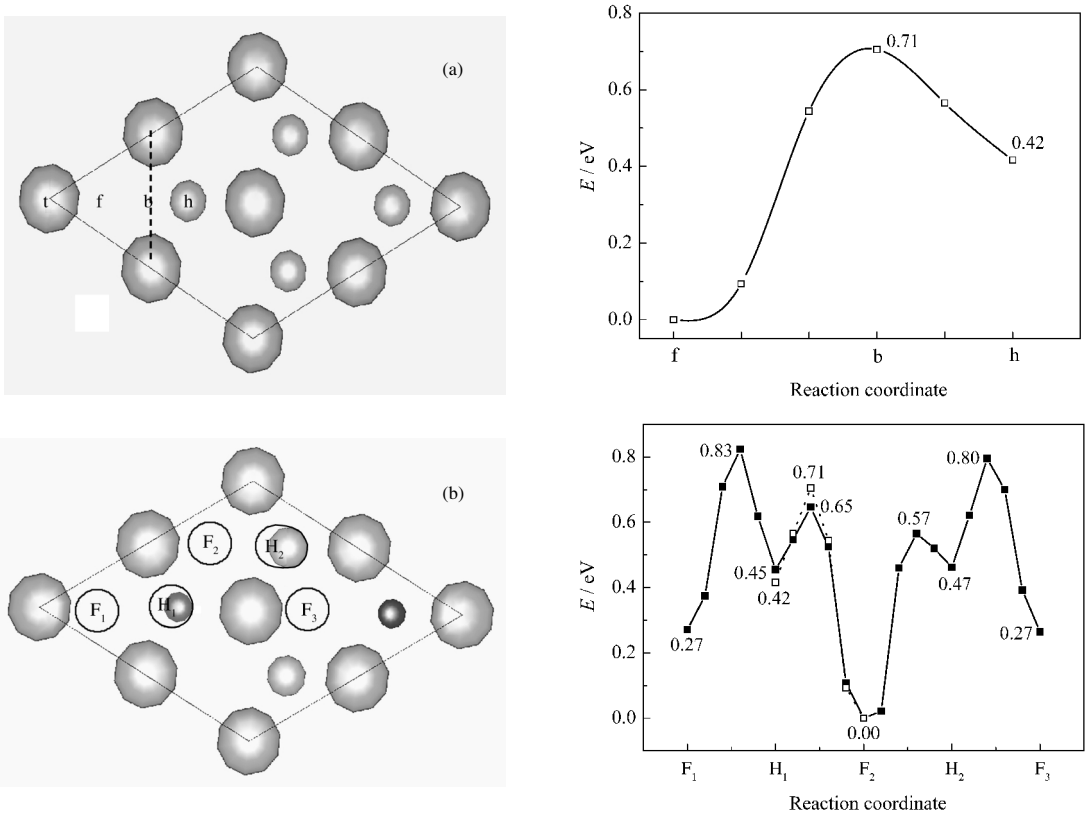

Fig.3 Calculated oxygen diffusion profile on the surfaces of (a) pure Pt(111), and (b) Pt-skin-$Pt_3Ni(111)$ by CI-NEB

F_3 is equivalent to F_1.

for the diffusion from F_2(PNN) to H_1(N) which is a little lower than that on the pure Pt(111) surface (0.71 eV). The other activation energies are about 0.56 eV from F_1(PPN) to H_1(N), 0.57 eV from F_2(PNN) to H_2(P), and 0.33 eV from H_2(P) to F_3(PPN). Therefore, on the Pt-skin-Pt_3Ni(111), the oxygen mobility would be much higher than that on the pure Pt(111) surface, which is correlated with the higher ORR efficiency on Pt-skin-Pt_3Ni(111). This explains quite well for the experimental observations that the Pt-skin-Pt_3Ni(111) is 10-fold more active for the ORR than the corresponding Pt(111) surface[2], since a barrier decrease of 0.1–0.2 eV can increase $\exp(-E_a/kT)$ by 10–100 times at 500 K, where E_a is the activation energy, k is Boltzmann′s constant, and T is temperature in Kelvin.

2.3 The bonding mechanism

From the above discussion, we are aware that the O adatom is bonded strongly at the fcc site, and the bridge site serves as a transition state for the O diffusion on the Pt(111) surface. Comparatively, Pt-skin-Pt_3Ni(111) surface has a weaker interaction and easier diffusion for the O adatom. In this part, the bonding mechanisms are studied through the electronic structure analyses, in order to have a better understanding to these conclusions.

Fig.4 shows the curves of partial density of state (PDOS) projected onto the 2*p* states of the O adatom and the 5*d* states for one of the Pt atoms bonded with the O adatom for O atom on the most favourable fcc hollow sites, as well as the bridge TS, on the Pt(111) and Pt-skin-Pt_3Ni(111) surfaces. The PDOS of Pt 5*d* for one of the Pt atoms on the clean Pt(111) and Pt-skin-Pt_3Ni(111) surfaces are also shown in the figure for comparison. Spin-polarized calculations are performed for all the systems, but only the DOS for the spin up channel is shown since DOSs for the two spin channels are almost identical for both O and Pt.

By examining the individual quantum states of the O adatom on the most favourable fcc hollow sites on the two surfaces, it is found that there is a sharp peak (not shown in the energy window in Fig.4) located at about 19.5 eV below the Fermi level which has almost exclusively O 2*s* character. The large intensity of the O 2*s* peak indicates a high localization of the O 2*s* electrons around the O adatom. The DOS peaks at about 6.5 eV below the Fermi level and those just above the Fermi level [the solid lines in Fig.4(a, b)], as well as the corresponding peaks at the same energy positions in the PDOS of Pt 5*d* [the solid lines in Fig.4(c, d)] originated from the interaction of the O 2*p* and Pt 5*d* states and correspond to the O 2*p*-Pt 5*d* bonding states (the peaks at about −6.5 eV) and antibonding states (the peaks just above the Fermi level), respectively. The very low intensities from −5.0 eV to the Fermi level [the solid lines in Fig.4(a, b)] indicate that almost all the O 2*p* electrons are used up by forming strong bonding with the Pt atoms around the fcc hollow site. Therefore, it is expected that the 2*p* states of the O atom on the fcc hollow site should be "saturated". The large separation between the bonding-antibonding states reflects the strong O-Pt interaction. Indeed, with the strong O-Pt interaction, the surface *d*-band for both the Pt(111) and Pt-skin-Pt_3Ni(111) are broadened with new peaks appeared corresponding the bonding (below the Pt 5*d* band) and antibonding states (above the Pt 5*d* band), respectively, as compared with the PDOS of Pt 5*d* for clean surfaces [the dotdashed lines in Fig. 4(c, d)].

In the case of O adatom on the bridge site as shown in Fig.4(a, b) (the dotted lines), however, the O 2*p* has a smaller bonding peak with higher energy and a larger antibonding peak with lower energy than those in the case of O on the fcc hollow site. The *p*-*d* antibonding states have significant densities near the Fermi level. Therefore, some O 2*p* orbitals are available to form new bonding and the O atom is reactive on the bridge site. The DOS features above, as well as the smaller bonding-antibonding states separation indicate that, once the O moves to a bridge site, the O 2*p* orbital does not mix strongly with Pt 5*d* states.

Because of the saturation of O 2*p* orbitals in the 3-fold fcc hollow site, the O atom is inactive. Thus it must be activated to a bridge site to form a transition state for oxygen diffusion. The relative smaller O 2*p* bonding state peak at the fcc site of Pt-skin-Pt_3Ni(111) surface as compared with that of the pure Pt(111) surface [c.f. the solid lines in Fig.4(a, b)] explains the weaker O adsorption on the Pt-skin-Pt_3Ni(111) surface. Therefore, on Pt-skin-Pt_3Ni(111) surface, the bonding of O 2*p*-Pt 5*d* is easier to be

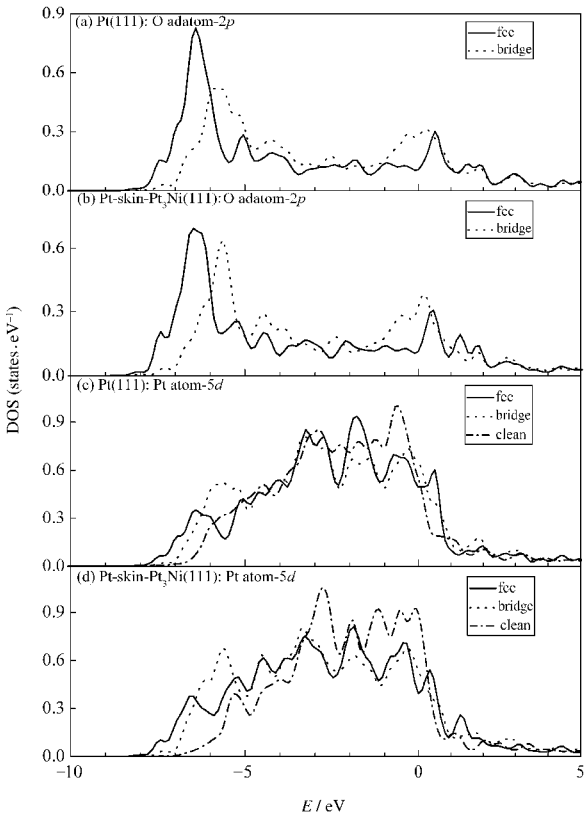

Fig.4 PDOSs of the 2*p* states of the O adatom and the 5*d* states for one of the Pt atoms bonded with the O adatom on the Pt(111) and Pt-skin-Pt_3Ni(111) surfaces for the most favourable fcc hollow site and the TS bridge site (bri) adsorption configurations

The PDOS of Pt 5*d* on the clean surfaces are also shown for comparison.

broken and the O adatom is easier to be activated to the bridge site than on the pure Pt(111) surface. This is why the surface of Pt-skin-$Pt_3Ni(111)$ has a higher oxygen diffusion activity than the surface of pure Pt(111).

3 Conclusions

The geometric and electronic structures of oxygen adsorption on the Pt-skin-$Pt_3Ni(111)$ surface were studied using first-principles methods based on the density functional theory. It is found that the most stable adsorption position of the oxygen on the Pt-skin-$Pt_3Ni(111)$ surface is the fcc site, but with a weaker adsorption as compared with that on the pure Pt(111) surface. The *d*-band of the Pt-skin in the Pt-skin-$Pt_3Ni(111)$ surface was broadened and lowered in energy (with a lower *d*-band center) as compared with that of the pure Pt(111) by the interaction with the subsurface Ni, which plays important roles in altering the catalytic properties of the Pt-skin-$Pt_3Ni(111)$.

The activation energies for oxygen diffusion were also examined. It is found that on Pt-skin-$Pt_3Ni(111)$ surface the maximum diffusion barrier (with the bridge site served as a transition state) is 0.65 eV, which is lower than that on the pure Pt(111) surface (0.71 eV), which explains quite well for the experimental observations that the Pt-skin-$Pt_3Ni(111)$ is much more active for the ORR than the corresponding Pt(111) surface.

References

1 Whitesides, G. M.; Crabtree, G. W. *Science*, **2007, 315**: 796

2 Stamenkovic, V. R.; Fowler, B.; Mun, B. S.; Wang, G.; Ross, P. N.; Lucas, C. A.; Markovic, N. M. *Science*, **2007, 315**: 493

3 Stamenkovic, V. R.; Mun, B. S.; Arenz, M.; Mayrhofer, K. J. J.; Lucas, C. A.; Wang, G.; Ross, P. N.; Markovic, N. M. *Nat. Mater*., **2007, 6**: 241

4 Mun, B. S.; Watanabe, M.; Rossi, M.; Stamenkovic, V.; Markovic, N. M.; Ross, P. N. *J. Chem. Phys*., **2005, 123**: 204717

5 Markovic, N. M.; Schmidt, T. J.; Stamenkovic, V.; Ross, P. N. *Fuel Cells*, **2001, 1**: 105

6 Zhang, J.; Vukmirovic, M. B.; Xu, Y.; Mavrikakis, M.; Adzic, R. R. *Angew. Chem. Int. Ed*., **2005, 44**: 2132

7 Jacob, T.; Goddard III, W. A. *J. Phys. Chem. B*, **2004, 108**: 8311

8 Su, H. Y.; Bao, X. H.; Li, W. X. *J. Chem. Phys*., **2008, 128**: 194707

9 Ma, Y.; Balbuena, P. B. *Surf. Sci*., **2008, 602**: 107

10 Kitchin, J. R.; Norskov, J. K.; Barteau, M. A.; Chen, J. G. *J. Chem. Phys*., **2004, 120**: 10240

11 Kitchin, J. R.; Norskov, J. K.; Barteau, M. A.; Chen, J. G. *Phys. Rev. Lett*., **2004, 93**: 156801

12 Nilekar, A. U.; Xu, Y.; Zhang, J.; Vukmirovic, M. B.; Sasaki, K.; Adzic, R. R.; Mavrikakis, M. *Top. Catal*., **2007, 46**: 276

13 Ma, Y.; Balbuena, P. B. *J. Phys. Chem. C*, **2008, 112**: 14520

14 Kittel, C.; McEuen, P. Introduction to solid state physics. New York: Wiley, 1986

15 Han, B. C.; Ceder, G. *Phys. Rev. B*, **2006, 74**: 205418

16 Xu, Y.; Ruban, A. V.; Mavrikakis, M. *J. Am. Chem. Soc*., **2004, 126**: 4717

17 Xu, J.; Saeys, M. *J. Phys. Chem. C*, **2008, 112**: 9679

18 Gauthier, Y. *Surf. Rev. Lett.*, **1996, 3**: 1663

19 Gauthier, Y.; Baudoing-Savois, R.; Bugnard, J. M.; Bardi, U.; Atrei, A. *Surf. Sci*., **1992, 276**: 1

20 Gauthier, Y.; Joly, Y.; Baudoing, R.; Rundgren, J. *Phys. Rev. B*, **1985, 31**: 6216

21 Lundberg, M. *Phys. Rev. B*, **1987, 36**: 4692

22 Kresse, G.; Furthmuller, J. *Comput. Mater. Sci*., **1996, 6**: 15

23 Kresse, G.; Hafner, J. *Phys. Rev. B*, **1993, 47**: 558

24 Blöchl, P. E. *Phys. Rev. B*, **1994, 50**: 17953

25 Monkhorst, H. J.; Pack, J. D. *Phys. Rev. B*, **1976, 13**: 5188

26 Henkelman, G.; Uberuaga, B. P.; Jónsson, H. *J. Chem. Phys*., **2000, 113**: 9901

27 Getman, R. B.; Schneider, W. F. *J. Phys. Chem. C*, **2007, 111**: 389

28 Gland, J. L.; Sexton, B. A.; Fisher, G. B. *Surf. Sci*., **1980, 95**: 587

29 Yeo, Y. Y. *J. Chem. Phys*., **1997, 106**: 392

30 Hammer, B.; Nörskov, J. K. *Adv. Catal*., **2000, 45**: 71

31 Greeley, J.; Nörskov, J. K.; Mavrikakis, M. *Annual Reviews in Physical Chemistry*, **2002, 53**: 319

32 Bleakley, K.; Hu, P. *J. Am. Chem. Soc*., **1999, 121**: 7644

33 Materer, N.; Starke, U.; Barbieri, A.; DoLl, R.; Heinz, K.; Van Hove, M. A.; Somorjai, G. A. *Surf. Sci*., **1995, 325**: 207

34 Mittendorfer, F.; Eichler, A.; Hafner, J. *Surf. Sci*., **1999, 433**: 756

35 Pedio, M.; Becker, L.; Hillert, B.; D′Addato, S.; Haase, J. *Phys. Rev. B*, **1990, 41**: 7462